China Ocean Eng., 2023, Vol. 37, No. 1, P. 29–41
DOI: https://doi.org/10.1007/s13344-023-0003-9, ISSN 0890-5487
http://www.chinaoceanengin.cn/ E-mail: coe@nhri.cn

Abandonment and Recovery Operation of Steel Lazy-Wave Riser in Deep-water by Controlled Vessel and Cable Velocity Rate

GU Ji-jun[a, *], HUANG Jun[b], GAO Lei[a, b], CHEN Lei-lei[a], JIA Ji-chuan[a], WANG Shu-jiang[a]

[a] College of Mechanical and Transportation Engineering, China University of Petroleum-Beijing, Beijing 102249, China

[b] CNOOC Research Institute, Beijing 100028, China

Received June 18, 2022; revised February 6, 2023; accepted February 20, 2023

Abstract

Evaluation of abandonment and recovery operation of steel lazy-wave riser in deepwater is presented in this paper. The calculation procedure includes two single continuous SLWR and cable segments, which are coupled together to form the overall mathematical model. Then the equilibrium equations of SLWR and cable are established based on minimum total potential energy principle. The coupled equations are discretized by the finite difference method and solved by Newton-Raphson technique in an iterative manner. The present method is validated by well-established commercial code OrcaFlex. Recovery methods by considering different ratios of vessel's moving velocity to cable's recovery velocity are evaluated to optimize the abandonment and recovery operation. In order to keep the tension more stable during the recovery process, the rate ratio before leaving the seabed is increased, and the rate ratio after leaving the seabed is reduced.

Key words: steel lazy-wave riser, abandonment, recovery

Citation: Gu, J.J., Huang, J., Gao, L., Chen, L.L., Jia, J.C., Wang, S.J., 2023. Abandonment and recovery operation of steel lazy-wave riser in deepwater by controlled vessel and cable velocity rate. China Ocean Eng., 37(1): 29–41, doi: https://doi.org/10.1007/s13344-023-0003-9

1 Introduction

The steel lazy wave riser (SLWR) is an oil and gas transportation system that connects the manifold on the seabed and the oil production floating platform (ex. offshore platform, floating production storage and offloading (FPSO), etc). It is very suitable for deep-water oil and gas developments because it is flexible enough to avoid strong vortex-induced vibration (Cabrera-Miranda and Paik, 2019; Chen et al., 2021; Cheng et al., 2020; Yang and Li, 2011; Hoffman et al., 2017; Kim and Kim, 2015; Thomas et al., 2010). Thus, the impact of the ocean current will be diminished and the SLWR's fatigue lifetime will be greatly improved. Meanwhile, SLWR has distributed buoyancy to realize wavy riser configuration, which decouples the production floating platform motions at the riser touch down point and provides better compliance in harsh environmental conditions to increase riser fatigue performance.

During the installation process, to decrease the process risk of the SLWR installation from the floating platform arrival uncertianty, a pre-abandonment-recovery-transfer method of the SLWR is chosen (Thomas et al., 2010). This lowers the requirement for long installation weather windows which is normally associated with direct transfer methods, more freedom to abandon the riser in case of adverse weather conditions and availablity for field development to continue in case of the late arrival of the floating platform. Successful installation of SLWR by this method to the floating platform requires the design of a suitable recovery layout taking into consideration the installation sequence and careful assessment of the risks involved particularly in terms of clearance and interference issues with floating platform mooring lines.

Many pieces of research have been performed on static and dynamic analysis of SLWR. For example, Wang and Duan (2015) presented a nonlinear model which could simulate the nonlinear mechanical behavior of SLWR under the effects of pipe-soil interaction, ocean current and internal flow. Trapper (2020a) proposed a static mathematical model of SLWR which considered the riser and buoyancy sections as a single continuous segment to conduct feasible numerical analysis. Kim and Kim (2015) studied the dynamic behaviors of conventional steel catenary riser (SCR) and lazy-wave SCR for FPSOs in deepwater, which proved that lazy-wave SCR is very useful for mitigating local dynamic buckling

Foundation item: This research was financially supported by the National Natural Science Foundation of China (Grant No. 52271299), and the Science Foundation of China University of Petroleum, Beijing (Grant No. 2462020YXZZ046).

*Corresponding author. E-mail: gu@cup.edu.cn

problem. Cheng et al. (2020) used a nonlinear finite element method to conduct a dynamic analysis of deepwater steel lazy wave riser with the internal flow and seabed interaction. Oh et al. (2020) used a multi-body dynamics simulation technique and a developed design framework for the SLWR shape design. Ruan et al. (2021) studied on fatigue damage optimization mechanism of deepwater SLWR based on multiple waveform serial arrangement.

For the research on the riser response caused by the tension change, Jensen et al. (2010) established the nonlinear dynamic equation of SCR in the J-type laying operation, and discussed the influence of the horizontal tension on the lay angle, lay back and the configuration of the riser. Xu et al. (2021) analyzed the influence of tension on the riser deformation in the reel laying by the finite element software ABAQUS. It can be seen that the change of tension will have an important impact on the deformation of the riser. However, most studies only analyzed and discussed the laying and installation of SCR risers, but have not conducted in-depth research on the changes in tension during the installation or recovery of SLWR risers.

The innovation of this paper lies in the presentation of an efficient calculation procedure and its successful application to perform a study of tension effect on the installation of SLWR. Recovery methods by considering different vessel's moving velocity and cable's recovery velocity are performed to evaluate which one is preferable in the recovery operation. In the next section, an overview and overall solution steps of the proposed SLWR mathematical model is fully introduced. In Section 3, by making use of the Minimum Total Potential Energy Principle (Surana and Reddy, 2016), the coupled static equilibrium equations of the SLWR and cable are formulated. The finite difference method is implemented to solve differential equations and Newton-Raphson iterative algorithm used to solve the coupled equations in Section 4. Next, in Section 5, the numerical calculation results are compared with OrcaFlex (commercial code) to verify the feasibility and accuracy of the present model. Then recovery methods of the recovery operation are performed to evaluate the tension effect on abandonment and recovery operation. Finally, the closing section presents the main conclusions.

2 Overview of the problem

The abandonment and recovery system of steel lazy-wave riser in deepwater is usually divided into three parts: SLWR, cable, and the vessel, as shown in Fig. 1. The cable connects the SLWR to the vessel; the lower end of SLWR is connected to the riser base attached to the seabed, and its upper end connected to the cable. The SLWR and cable are coupled during the operation of abandonment and recovery from the initial to the final configuration. The pull-in wire is used to transfer the SLWR to the floating platform.

The present study establishes the mathematical model

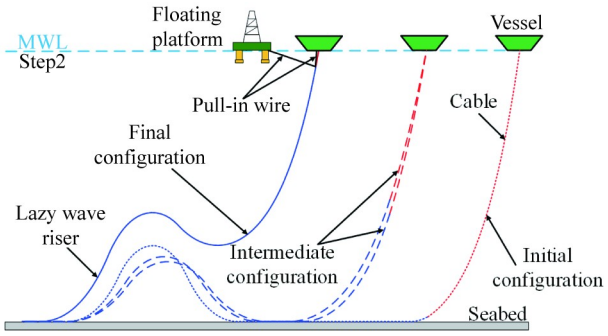

Fig. 1. Typical configuration of the SLWR during abandonment and recovery.

based on the following assumptions:

(1) All forces and ocean current directions act on the same plane, leading to a two-dimensional problem.

(2) Torsion, side bending and shear force are not considered.

(3) The riser and cable are treated as inextensible beam model.

(4) The riser is fully filled with seawater.

The overall static analysis of the abandonment and recovery is divided into two steps, as shown in Fig. 2 and Fig. 3.

Step 1. Solving the abandoned configuration of SLWR

The first step solves the initial position of SLWR. The initial configuration is assumed to be a straight line lying on the seabed, which is the abandoned configuration of SLWR. Then, the SLWR bends continuously under the action of buoyancy with the horizontal tension P_0 at the right end and

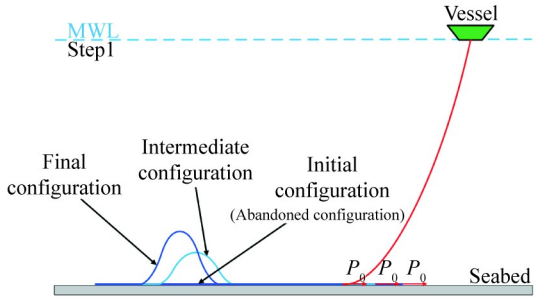

Fig. 2. Solution of the abandoned configuration of SLWR.

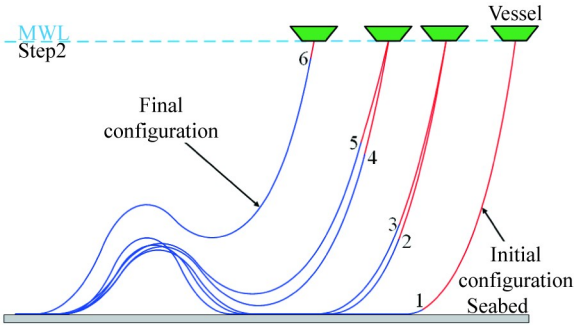

Fig. 3. Static equilibrium configuration of SLWR.

keeps constant; finally, it reaches the final configuration, as shown in Fig. 2. In the calculation process, the spring is used to simulate the seabed support force.

Step 2. Solving the static equilibrium configuration

The second step is to solve the overall static equilibrium configurations of the cable and SLWR. The static equilibrium means that the extreme value of the total potential energy of SLWR and cable is minimized, which is based on the principle of minimum potential energy to find the partial derivative of the potential energy equation and make the partial derivative equal to 0, so as to obtain the static equilibrium of SLWR and cable. First, the cable and SLWR are solved respectively, and then coupled together at the joint. In solving the static equilibrium configurations, the initial configuration of SLWR in the second step will be the final configuration calculated in the first step, and the abandoned configuration of cable will be the free catenary configuration. Finally, in order to determine the final configuration, both of the horizontal tension and vertical tension need to be considered for the cable and SLWR at the joint point.

At the beginning, the free end coordinates of the cable and SLWR do not coincide. The horizontal tension (P_0) and vertical buoyancy (F_C) of the free end must be adjusted continuously according to the error of horizontal and vertical distance until the coordinates of the cable and SLWR free end coincide.

The dynamic installation process of SLWR can be realized by changing the length of the cable and the position of the installation ship continuously, and solving the overall static equilibrium configuration of each cable length and the position of the installation ship in Step 2.

3 Mathematical model

Most of the previous studies usually divide the riser model into several sections, i.e. lower section, buoyancy section, upper section, and consider each section separately by applying continuity boundary conditions. Then the governing equations for each section are separated due to different gravity forces, which makes the governing equations complicated (Wang et al., 2014, 2015a, 2015b). In order to simplify the governing equations and deal with complicated boundary conditions during the installation process of SLWR, a new calculation procedure based on the minimization of the total potential energy of the system is proposed in the present study to handle the static analysis of SLWR and cable from abandonment and recovery winch. This method does not need to consider each section of the riser separately with compatibility conditions and will consider the whole riser as a single continuous section. The model is very flexible to deal with new loads, constraints, or boundary conditions to decide which SLWR geometry is preferable in certain conditions by easily conducting sensitivity analyses (Trapper, 2019, 2020a, 2020b; Trapper and Mishal, 2020; Chen et al., 2023; Gu et al., 2021).

The calculation model is established in the global coordinate system, where the origin point of the cable is set at the top right corner of the domain and the origin of the SLWR is set at the bottom left corner of the domain, as shown in Fig. 4. The MWL represents the mean water line. In both coordinate systems, the x-axis points to the right and the y-axis upwards from the seabed.

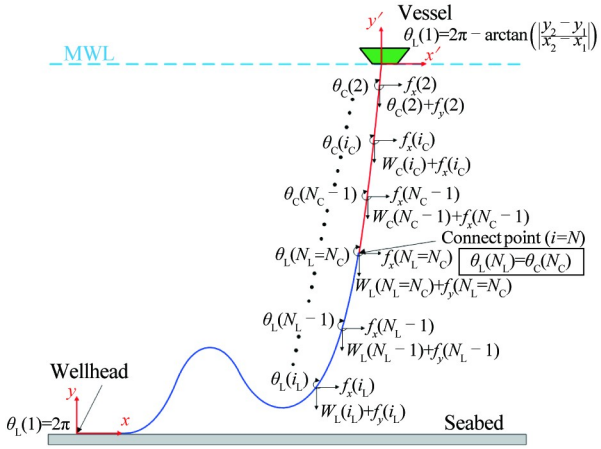

Fig. 4. Establishment of global coordinate system.

In the following equations, the subscript L refers to the SLWR, while subscript C refers to the cable. The SLWR and the cable are subjected to distributed submersed gravity w_L and w_C which act along the entire length of the pipe. Both of them are subjected to horizontal tension P_0 and vertical tension F_C at the connection point.

The connection point is used as the starting point of SLWR length and cable length, defining the SLWR's segment angle from θ_L (1) to θ_L (N_L) at each point of SLWR and the cable's segment angle from θ_C (1) to θ_C (N_C) at each point of cable, respectively. In Fig. 4, i_C represents the node sequence of cable, and i_L represents the node sequence of riser.

As SLWR and cable have their own starting coordinate systems, the boundary conditions for SLWR and cable are:

$$x_C(L_C) = 0; \tag{1}$$

$$y_C(L_C) = 0; \tag{2}$$

$$x_L(L_L) = 0; \tag{3}$$

$$y_L(L_L) = 0, \tag{4}$$

where, x_C is x coordinate of cable, L_C is length of cable, and y_C is y coordinate of cable. x_L is x coordinate of SLWR, L_L is length of SLWR, and y_L is y coordinate of SLWR.

Eqs. (1)−(4) are the end points corresponding to the upper right corner of the cable and the lower left corner of the riser, which are the origin point for the cable and SLWR respectively. The movements of the riser in the x and y directions at these two points are 0, i.e., both horizontal and vertical displacement constraints are set.

The configurations of SLWR and cable are set in the

Cartesian coordinate system x and y. Their relationships with the angle θ are given as follows, where s ($0<s<L$) is the length of a segment along the direction of the riser (Trapper, 2019):

$$x_{\mathrm{C}}(s_{\mathrm{C}}) = -\int_{s_{\mathrm{C}}}^{L_{\mathrm{C}}} \cos\theta_{\mathrm{C}}\left(s'_{\mathrm{C}}\right)\mathrm{d}s_{\mathrm{C}}; \tag{5}$$

$$y_{\mathrm{C}}(s_{\mathrm{C}}) = \int_{s_{\mathrm{C}}}^{L_{\mathrm{C}}} \sin\theta_{\mathrm{C}}\left(s'_{\mathrm{C}}\right)\mathrm{d}s_{\mathrm{C}}; \tag{6}$$

$$x_{\mathrm{L}}(s_{\mathrm{L}}) = \int_{s_{\mathrm{L}}}^{L_{\mathrm{L}}} \cos\theta_{\mathrm{L}}\left(s'_{\mathrm{L}}\right)\mathrm{d}s_{\mathrm{L}}; \tag{7}$$

$$y_{\mathrm{L}}(s_{\mathrm{L}}) = -\int_{s_{\mathrm{L}}}^{L_{\mathrm{L}}} \sin\theta_{\mathrm{L}}\left(s'_{\mathrm{L}}\right)\mathrm{d}s_{\mathrm{L}}, \tag{8}$$

where, s_{C} is the segment length of cable, and s_{L} is the segment length of SLWR.

Next, the SLWR and the cable configurations are established in the same coordinate system. At this stage, the coordinate transformation of the cable is required as follows:

$$x'_{\mathrm{C}} = -\int_{s_{\mathrm{C}}}^{L_{\mathrm{C}}} \cos\theta_{\mathrm{C}}(s'_{\mathrm{C}})\mathrm{d}s_{\mathrm{C}} + L_{\mathrm{span}}; \tag{9}$$

$$y'_{\mathrm{C}} = \int_{s_{\mathrm{C}}}^{L_{\mathrm{C}}} \sin\theta_{\mathrm{C}}(s'_{\mathrm{C}})\mathrm{d}s_{\mathrm{C}} + d_{\mathrm{w}}, \tag{10}$$

where, x'_{C}-y'_{C} refers to the same coordinate system after coordinate transformation.

The equilibrium equations of SLWR and cable will be established by adopting the *Minimum Total Potential Energy Principle* (Surana and Reddy, 2016). In a static case, the equilibrium position is achieved by assessing the minimization of total potential energy consisting of elastic strain energy of the deformed body and the potential energy of applied forces. It should be noted that the spring support force (stiffness K_{s}) is introduced to simulate the seabed stiffness, so that the riser shape is more in line with the actual situation.

Consider the bending of the beam as an elastic problem, the potential energy of the system is set to take the minimum value based on the principle of minimum potential energy (Dow, 1999), $\min_{\hat{u}_i\in BC(u)}\pi$. Among them, $\pi = U - W = \frac{1}{2}\int \sigma_{ij}\varepsilon_{ij}\mathrm{d}\Omega - \left(\int b_i u_i \mathrm{d}\Omega + \int p_i u_i \mathrm{d}A\right)$, the first term on the right side of the equation represents the internal elastic potential energy of the system, and the second term in parentheses represents the external work . The system potential energies of the SLWR segment and the cable segment are $\pi = U_{\mathrm{L}}$ and $\pi = U_{\mathrm{C}}$, respectively.

For SLWR, the elastic potential energy is $U_{\mathrm{L}} = \frac{1}{2}\int_{L_{\mathrm{L}}} E_{\mathrm{L}} I_{\mathrm{L}} \kappa_{\mathrm{L}}(s_{\mathrm{L}})^2 \mathrm{d}s_{\mathrm{L}}$, and the external work is $W_{\mathrm{L}} = \frac{1}{2}k_s e(s_{\mathrm{L}})^2 - \int_{L_{\mathrm{L}}} w_{\mathrm{L}} y_{\mathrm{L}}(s_{\mathrm{L}})\mathrm{d}s_{\mathrm{L}} - \int_{L_{\mathrm{L}}} f_{x_{\mathrm{L}}} x_{\mathrm{L}}(s_{\mathrm{L}})\mathrm{d}s_{\mathrm{L}} - \int_{L_{\mathrm{L}}} f_{y_{\mathrm{L}}} y_{\mathrm{L}}(s_{\mathrm{L}})\mathrm{d}s_{\mathrm{L}} + P_0 x_{\mathrm{L}}(L_{\mathrm{L}})$.

For cable, the elastic potential energy is $U_{\mathrm{C}} = \frac{1}{2}\int_{L_{\mathrm{C}}} E_{\mathrm{C}} I_{\mathrm{C}} \kappa_{\mathrm{C}}(s_{\mathrm{C}})^2 \mathrm{d}s_{\mathrm{C}}$, and the external work is $W_{\mathrm{C}} = -\int_{L_{\mathrm{C}}} w_{\mathrm{C}} y_{\mathrm{C}}(s_{\mathrm{C}})\mathrm{d}s_{\mathrm{C}} + \int_{L_{\mathrm{C}}} f_{x_{\mathrm{C}}} x_{\mathrm{C}}(s_{\mathrm{C}})\mathrm{d}s_{\mathrm{C}} - \int_{L_{\mathrm{C}}} f_{y_{\mathrm{C}}} y_{\mathrm{C}}(s_{\mathrm{C}})\mathrm{d}s_{\mathrm{C}} - P_0 x_{\mathrm{C}}(L_{\mathrm{C}}) - F_{\mathrm{C}} y_{\mathrm{C}}(L_{\mathrm{C}})$.

Referring to the definition of the total potential energy of the system by Trapper (2019, 2020a, 2020b), the equilibrium equation established for SLWR is:

Step 1: SLWR is subjected to horizontal tension.

$$\begin{aligned} U_{\mathrm{L}} = {} & \frac{1}{2}\int_{L_{\mathrm{L}}} E_{\mathrm{L}} I_{\mathrm{L}} \kappa_{\mathrm{L}}(s_{\mathrm{L}})^2 \mathrm{d}s_{\mathrm{L}} - \frac{1}{2}k_{\mathrm{s}} e(s_{\mathrm{L}})^2 + \\ & \int_{L_{\mathrm{L}}} w_{\mathrm{L}} y_{\mathrm{L}}(s_{\mathrm{L}})\mathrm{d}s_{\mathrm{L}} - \int_{L_{\mathrm{L}}} f_{x_{\mathrm{L}}} x_{\mathrm{L}}(s_{\mathrm{L}})\mathrm{d}s_{\mathrm{L}} + \\ & \int_{L_{\mathrm{L}}} f_{y_{\mathrm{L}}} y_{\mathrm{L}}(s_{\mathrm{L}})\mathrm{d}s_{\mathrm{L}} - P_0 x_{\mathrm{L}}(L_{\mathrm{L}}). \end{aligned} \tag{11}$$

Step 2: SLWR is not only subjected to horizontal tension, but also vertical tension provided by the cable.

$$\begin{aligned} U_{\mathrm{L}} = {} & \frac{1}{2}\int_{L_{\mathrm{L}}} E_{\mathrm{L}} I_{\mathrm{L}} \kappa_{\mathrm{L}}(s_{\mathrm{L}})^2 \mathrm{d}s_{\mathrm{L}} - \frac{1}{2}\int_{L_{\mathrm{L}}} k_{\mathrm{s}} e(s_{\mathrm{L}})^2 \mathrm{d}s_{\mathrm{L}} + \\ & \int_{L_{\mathrm{L}}} w_{\mathrm{L}} y_{\mathrm{L}}(s_{\mathrm{L}})\mathrm{d}s_{\mathrm{L}} - \int_{L_{\mathrm{L}}} f_{x_{\mathrm{L}}} x_{\mathrm{L}}(s_{\mathrm{L}})\mathrm{d}s_{\mathrm{L}} + \\ & \int_{L_{\mathrm{L}}} f_{y_{\mathrm{L}}} y_{\mathrm{L}}(s_{\mathrm{L}})\mathrm{d}s_{\mathrm{L}} - P_0 x_{\mathrm{L}}(L_{\mathrm{L}}) - F_{\mathrm{C}} y_{\mathrm{L}}(L_{\mathrm{L}}). \end{aligned} \tag{12}$$

The equilibrium equation established for cable is:

$$\begin{aligned} U_{\mathrm{C}} = {} & \frac{1}{2}\int_{L_{\mathrm{C}}} E_{\mathrm{C}} I_{\mathrm{C}} \kappa_{\mathrm{C}}(s_{\mathrm{C}})^2 \mathrm{d}s_{\mathrm{C}} + \int_{L_{\mathrm{C}}} w_{\mathrm{C}} y_{\mathrm{C}}(s_{\mathrm{C}})\mathrm{d}s_{\mathrm{C}} - \\ & \int_{L_{\mathrm{C}}} f_{x_{\mathrm{C}}} x_{\mathrm{C}}(s_{\mathrm{C}})\mathrm{d}s_{\mathrm{C}} + \int_{L_{\mathrm{C}}} f_{y_{\mathrm{C}}} y_{\mathrm{C}}(s_{\mathrm{C}})\mathrm{d}s_{\mathrm{C}} + \\ & P_0 x_{\mathrm{C}}(L_{\mathrm{C}}) + F_{\mathrm{C}} y_{\mathrm{C}}(L_{\mathrm{C}}). \end{aligned} \tag{13}$$

In Eqs. (11)–(13), the first term represents the bending elastic energy stored in SLWR and cable. The solution does not consider the axial extension of the riser, but only the planar deformation of the riser. Thus only the bending strain is considered.

Define κ as the planar curvature and I as the moment of inertia of the SLWR or cable, and they are given by:

$$\kappa(s_{\mathrm{L}}) = \frac{\mathrm{d}\theta_{\mathrm{L}}(s_{\mathrm{L}})}{\mathrm{d}s_{\mathrm{L}}}; \tag{14}$$

$$I = \frac{\pi}{4}\left[\left(\frac{D}{2}\right)^4 - \left(\frac{D}{2} - t\right)^4\right]. \tag{15}$$

The second term in Eqs. (11) and (12) represents the elastic energy stored in the deformation of elastic seabed, and $e(s_{\mathrm{L}})$ represents the sinking depth of the free end of SLWR, which is:

$$k_{\mathrm{s}}(i) = \begin{cases} k_{\mathrm{s}}\Delta s_{\mathrm{L}}, & y_{\mathrm{L}}(i) \geqslant d_{\mathrm{w}} \\ 0, & y_{\mathrm{L}}(i) < d_{\mathrm{w}} \end{cases} \tag{16}$$

$$e(s_{\mathrm{L}}) = e\left[y_{\mathrm{L}}(s_{\mathrm{L}})\right] = \begin{cases} y_{\mathrm{L}}(s_{\mathrm{L}}) - d_{\mathrm{w}}, & y_{\mathrm{L}}(s_{\mathrm{L}}) \geqslant d_{\mathrm{w}} \\ 0, & y_{\mathrm{L}}(s_{\mathrm{L}}) < d_{\mathrm{w}} \end{cases} \tag{17}$$

where, d_{w} is the water depth of the left end of SLWR.

We assume that there is no suction force in a case of separation (Randolph and Gourvenec, 2011). Then, the seabed support reaction (per unit length) is given by:

$$R_{\mathrm{s}}(s_{\mathrm{L}}) = k_{\mathrm{s}} e(s_{\mathrm{L}}). \tag{18}$$

The third term in Eqs. (11)–(12) or second term in Eq.

(13) represents the potential energy of submerged self-weight of SLWR and cable, obtained as follows:

$$w = (\rho - \rho_s) gA, \tag{19}$$

where, A is the cross-sectional area of the riser:

$$A = \pi\left[\left(\frac{D}{2}\right)^2 - \left(\frac{D}{2} - t\right)^2\right]. \tag{20}$$

But for SLWR, at the buoy position, the gravity is:

$$w_L(s_L) = w_L + \begin{cases} w_B, & s_L \in L_b \\ 0, & s_L \notin L_b \end{cases} \tag{21}$$

The fourth and fifth terms in Eqs. (11)−(12) and third and fourth terms in Eq. (13) represent the potential energy of distributed loads, f_x and f_y in x and y directions respectively due to ocean current. Morison's equations (Morison et al., 1950) are adopted to yield the force of ocean current as follows:

$$f_n = -\frac{1}{2}\rho_s C_n D |v_x(y)\sin\theta| v_x(y)\sin\theta; \tag{22}$$

$$f_\tau = \frac{1}{2}\rho_s C_\tau D |v_x(y)\cos\theta| v_x(y)\cos\theta. \tag{23}$$

The normal and tangential forces of the current, which acting on the riser need to be converted into the x and y directions:

$$f_x = -f_n\sin\theta + f_\tau\cos\theta; \tag{24}$$

$$f_y = f_n\cos\theta + f_\tau\sin\theta. \tag{25}$$

The sixth term in Eqs. (11)−(12) or fifth term in Eq. (13) represents the potential energy of the horizontal pulling force, P_0. It should be noted that the forces involved in Eqs. (22)−(25) are loads of per unit length.

The last term in Eqs. (12)−(13) represents the potential energy of the vertical pulling force, F_C.

Once the equilibrium equations are established and θ determined, the bending moment, shear force and axial tension of SLWR and cable can be solved by:

$$M(s) = EI\kappa(s); \tag{26}$$

$$S(s) = -\frac{\mathrm{d}M(s)}{\mathrm{d}s}; \tag{27}$$

$$T(s) = \int f_x\cos\theta(s)\mathrm{d}s - \int \left\{\left[f_y + w(s)\right]\sin\theta(s)\right\}\mathrm{d}s. \tag{28}$$

The value of the tension at each node is calculated by element discretization, and integrated to obtain the tension $T(s)$ by the length $\mathrm{d}s$. It should be noted that θ is not distinguishable for SLWR and cable in Eqs. (14)−(25).

4 Numerical implementation

4.1 Finite difference discretization

4.1.1 *Finite difference discretization of SLWR*

SLWR and cable lines are discretized into N−1 segments each, and the Finite Difference Method (Chatjigeorgiou, 2004; Kuiper et al., 2008) is implemented to discretize Eqs. (11)−(13). At the initial boundary points of riser and cable, assuming that the two ends of the structure are hinged, the motion of the SLWR initial node should be zero, the motion of the top node of the cable remains unchanged relative to the ship, and the bending moment at both ends should be equal to zero.

$$\begin{cases} u_i(L_L, L_C) = 0 \\ v_i(L_L, L_C) = 0 \\ EI\kappa_i(L_L, L_C) = 0 \end{cases} \tag{29}$$

Table 1 Basic parameters

Parameter	Symbol	Value
SLWR's outer diameter (m)	D_L	0.2032
SLWR's wall thickness (m)	t_L	0.0191
SLWR's density (m³/s)	ρ_L	7860
SLWR's elasticity modulus (N/m²)	E_L	2.06×10^{11}
Moment of inertia of SLWR's cross-section (kg·m²)	I_L	
Planar curvature radius of SLWR's cross-section (m)	κ_L	
Planar curvature radius of cable's cross-section (m)	κ_C	
Wetted gravity load of SLWR (N/m)	w_L	
Wetted gravity load of cable (N/m)	w_C	
Buoyance can's outer diameter (m)	D_B	0.4
Buoyance can's density (m³/s)	ρ_B	116.67
Buoyance can's weight (kg)	w_B	
Cable's diameter (m)	D_C	0.102
Cable's density (m³/s)	ρ_C	7860
Cable's elasticity modulus (N/m²)	E_C	1.5319×10^8
The moment of inertia of cable's cross-section (kg·m²)	I_C	
Cross-sectional area of the riser (m²)	A	
Seawater density (m³/s)	ρ_s	1024
Normal drag coefficient	C_n	1.2
Tangential drag coefficient	C_τ	0.24
Horizontal component of top tension (N)	P_0	
Water depth (m)	d_w	1600
Span length (m)	L_{span}	
SLWR's segment length (m)	s_L	
SLWR's length (m)	L_L	
SLWR's segment angle (°)	θ_L	
Cable's segment length (m)	s_C	
Cable's length (m)	L_C	
Cable's segment angle (°)	θ_C	
SLWR's node number	N_L	
Cable's node number	N_C	
Spring stiffness (N/m)	k_s	4000
Vertical component of top tension (N)	F_C	
Horizontal component of current force (N)	f_x	Variable
Vertical component of current force (N)	f_y	Variable
Normal force due to current acting on riser (N)	f_n	Variable
Tangential force due to current acting on riser (N)	f_τ	Variable
Sinking depth (m)	e	
Seabed support reaction (per unit length) (N)	R_s	
Bending moment (kN·m)	M	Variable
Shear force (kN)	S	Variable
Axial tension (kN)	T	Variable
Seabed stiffness (N/m)	k_{SB}	

where, u is horizonal displacement and v is vertical displacement of SLWR and cable. Besides, the central difference is considered on the intermediate nodes. Generate 3 sets of N coupled equations for SLWR and cable, as follows:

SLWR:

Step 1:

$$U_{\mathrm{L}} = \Delta s_{\mathrm{L}} \sum_{i=2}^{N_{\mathrm{L}}} \frac{1}{2} E_{\mathrm{L}} I_{\mathrm{L}} \left[\frac{\theta_{\mathrm{L}}(i+1) - \theta_{\mathrm{L}}(i-1)}{2\Delta s_{\mathrm{L}}} \right]^2 - \sum_{i=1}^{N_{\mathrm{L}}+1} \frac{1}{2} k_{\mathrm{SB}}(i) \left[y_{\mathrm{L}}(i) - d_{\mathrm{w}} \right]^2 + \sum_{i=1}^{N_{\mathrm{L}}+1} w_{\mathrm{L}}(i) y_{\mathrm{L}}(i) - \sum_{i=1}^{N_{\mathrm{L}}+1} f_{x_{\mathrm{L}}}(i) x_{\mathrm{L}}(i) + \sum_{i=1}^{N_{\mathrm{L}}+1} f_{y_{\mathrm{L}}}(i) y_{\mathrm{L}}(i) - P_0 x_{\mathrm{L}}(1). \tag{30}$$

Step 2:

$$U_{\mathrm{L}} = \Delta s_{\mathrm{L}} \sum_{i=2}^{N_{\mathrm{L}}} \frac{1}{2} E_{\mathrm{L}} I_{\mathrm{L}} \left[\frac{\theta_{\mathrm{L}}(i+1) - \theta_{\mathrm{L}}(i-1)}{2\Delta s_{\mathrm{L}}} \right]^2 - \sum_{i=1}^{N_{\mathrm{L}}+1} \frac{1}{2} k_{\mathrm{SB}}(i) \left[y_{\mathrm{L}}(i) - d_{\mathrm{w}} \right]^2 + \sum_{i=1}^{N_{\mathrm{L}}+1} w_{\mathrm{L}}(i) y_{\mathrm{L}}(i) - \sum_{i=1}^{N_{\mathrm{L}}+1} f_{x_{\mathrm{L}}}(i) x_{\mathrm{L}}(i) + \sum_{i=1}^{N_{\mathrm{L}}+1} f_{y_{\mathrm{L}}}(i) y_{\mathrm{L}}(i) - P_0 x_{\mathrm{L}}(1) - F_{\mathrm{C}} y_{\mathrm{L}}(1). \tag{31}$$

4.1.2 *Finite difference discretization of cable*

$$U_{\mathrm{C}} = \Delta s_{\mathrm{C}} \sum_{i=2}^{N_{\mathrm{C}}} \frac{1}{2} E_{\mathrm{C}} I_{\mathrm{C}} \left[\frac{\theta_{\mathrm{C}}(i+1) - \theta_{\mathrm{C}}(i-1)}{2\Delta s_{\mathrm{C}}} \right]^2 + \sum_{i=1}^{N_{\mathrm{C}}+1} w_{\mathrm{C}} y_{\mathrm{C}}(i) - \sum_{i=1}^{N_{\mathrm{C}}+1} f_{x_{\mathrm{C}}}(i) x_{\mathrm{C}}(i) + \sum_{i=1}^{N_{\mathrm{C}}+1} f_{y_{\mathrm{C}}}(i) y_{\mathrm{C}}(i) + P_0 x_{\mathrm{C}}(1) + F_{\mathrm{C}} y_{\mathrm{C}}(1), \tag{32}$$

where, SLWR is divided into $N_{\mathrm{L}}+1$ nodes and N_{L} segments, with length equal to $\Delta s_{\mathrm{L}} = L_{\mathrm{L}}/N_{\mathrm{L}}$;

Cable is divided into $N_{\mathrm{C}}+1$ nodes, N_{C} segments, with length equal to $\Delta s_{\mathrm{C}} = L_{\mathrm{C}}/N_{\mathrm{C}}$;

Among them, the forward difference order on the boundary is the first order difference, and the central difference order on the non-boundary is the second order difference (Hoffman and Frankel, 2001; Ismail-Zadeh and Tackley, 2010; Wang et al., 2018).

For the SLWR section, the initial node is the left boundary point of the SLWR, and the boundary conditions are known as $\theta_{\mathrm{L}}(1) = 2\pi$. Therefore, the boundary difference of κ can be expressed as $\kappa(s_{\mathrm{L}}) = \dfrac{\theta_{\mathrm{L}}(i+1) - \theta_{\mathrm{L}}(i)}{\Delta s_{\mathrm{L}}}$, $i = 1$.

For the cable section, the initial node is the boundary point at the right end of the cable, and the boundary condition is known as $\theta_{\mathrm{C}}(i) = 2\pi - \arctan\left(\left| \dfrac{y_{i+1} - y_i}{x_{i+1} - x_i} \right| \right)$, $i = 1$. In the MATLAB program, the point is obtained by changing the x-y coordinate value. Therefore, the boundary difference of κ can be expressed as $\kappa(s_{\mathrm{C}}) \dfrac{\theta_{\mathrm{C}}(i+1) - \theta_{\mathrm{C}}(i)}{\Delta s_{\mathrm{C}}}$, $i = 1$.

The generalized gravity force acting at each SLWR and cable node is given by

$$w(i) = w\Delta s. \tag{33}$$

The hydrodynamic drag forces are discretized by:

$$f_n(i) = -\frac{1}{2} \rho_{\mathrm{s}} C_n D \Delta s \left| v_x(i) \sin\theta(i) \right| v_x(i) \sin\theta(i); \tag{34}$$

$$f_\tau(i) = \frac{1}{2} \rho_{\mathrm{s}} C_\tau D \Delta s \left| v_x(i) \cos\theta(i) \right| v_x(i) \cos\theta(i). \tag{35}$$

Then the force acting on the SLWR and cable in the x and y directions are expressed in discretized forms

$$f_x(i) = -f_n(i) \sin\theta(i) + f_\tau(i) \cos\theta(i); \tag{36}$$

$$f_y(i) = f_n(i) \cos\theta(i) + f_\tau(i) \sin\theta(i). \tag{37}$$

According to the coordinate system established in Fig. 4, the coordinate of each node of SLWR is represented by θ_{L}, and the difference format of x_{L} and y_{L} can be obtained

$$x_{\mathrm{L}}(i) = \sum_{j=i}^{N_{\mathrm{L}}} \cos\theta_{\mathrm{L}}(j) \Delta s_{\mathrm{L}}; \tag{38}$$

$$y_{\mathrm{L}}(i) = -\sum_{j=i}^{N_{\mathrm{L}}} \sin\theta_{\mathrm{L}}(j) \Delta s_{\mathrm{L}}. \tag{39}$$

In the same way, the coordinate of each node on the cable is represented by θ_{C}, and the difference format of x_{C} and y_{C} can be obtained as:

$$x_{\mathrm{C}}(i) = -\sum_{j=i}^{N_{\mathrm{C}}} \cos\theta_{\mathrm{C}}(j) \Delta s_{\mathrm{C}}; \tag{40}$$

$$y_{\mathrm{C}}(i) = \sum_{j=i}^{N_{\mathrm{C}}} \sin\theta_{\mathrm{C}}(j) \Delta s_{\mathrm{C}}. \tag{41}$$

In order to find the equilibrium configuration based on *Minimum total potential energy principle*, Eqs. (11)−(13) need to be derivated with respect to variable θ and equal to 0, yields

$$\frac{\partial U(\theta(1), \theta(2), \cdots, \theta(N))}{\partial \theta(i)} = 0,\ i = 1, 2, \cdots, N. \tag{42}$$

Eq. (41) contains N equations with respect to N unknown variables $(\theta(1), \theta(2), \cdots, \theta(N))$.

Put Eqs. (30)−(32) into Eq. (41) for derivation, and then substitute Eqs. (33)−(40) into Eqs. (30)−(32) to obtain the final solution forms. Since the boundary conditions are given above, Eqs. (43), (44) and (46) are the derivatives of discrete SLWR and cable non-boundary parts.

SLWR:

Step 1:

$$-\frac{1}{2}\frac{E_{\mathrm{L}}I_{\mathrm{L}}}{2\Delta s_{\mathrm{L}}}\left[\theta_{\mathrm{L}}(i+2)-\theta_{\mathrm{L}}(i)\right]+\sum_{j=1}^{i}k_{\mathrm{SB}}(j)\left\{\left[-\sum_{k=j}^{N}\Delta s_{\mathrm{L}}\sin\theta_{\mathrm{L}}(k)\right]-d_{\mathrm{w}}\right\}\Delta s_{\mathrm{L}}\cos\theta_{\mathrm{L}}(i)+\sum_{j=i+1}^{N+1}f_{x_{\mathrm{L}}}(i)\Delta s_{\mathrm{L}}\sin\theta_{\mathrm{L}}(i)-\sum_{j=1}^{i}\left[f_{y_{\mathrm{L}}}(j)+w_{\mathrm{L}}(j)\right]\Delta s_{\mathrm{L}}\cos\theta_{\mathrm{L}}(i)-P_0\left[\Delta s_{\mathrm{L}}\sin\theta_{\mathrm{L}}(i)\right]=0. \tag{43}$$

Step 2:

$$-\frac{1}{2}\frac{E_{\mathrm{L}}I_{\mathrm{L}}}{2\Delta s_{\mathrm{L}}}\left[\theta_{\mathrm{L}}(i+2)-\theta_{\mathrm{L}}(i)\right]+\sum_{j=1}^{i}k_{\mathrm{SB}}(j)\left\{\left[-\sum_{k=j}^{N}\Delta s_{\mathrm{L}}\sin\theta_{\mathrm{L}}(k)\right]-d_{\mathrm{w}}\right\}\Delta s_{\mathrm{L}}\cos\theta_{\mathrm{L}}(i)+\sum_{j=i+1}^{N+1}f_{x_{\mathrm{L}}}(i)\Delta s_{\mathrm{L}}\sin\theta_{\mathrm{L}}(i)-\sum_{j=1}^{i}\left[f_{y_{\mathrm{L}}}(j)+w_{\mathrm{L}}(j)\right]\Delta s_{\mathrm{L}}\cos\theta_{\mathrm{L}}(i)-P_0\left[\Delta s_{\mathrm{L}}\sin\theta_{\mathrm{L}}(i)\right]+F_{\mathrm{C}}\left[\Delta s_{\mathrm{L}}\cos\theta_{\mathrm{L}}(i)\right]=0, \tag{44}$$

where,

$$\sum_{j=1}^{i}k_{\mathrm{SB}}(i)\left[\sum_{k=j}^{N}\Delta s_{\mathrm{L}}\sin\theta_{\mathrm{L}}(k)\right]=\sum_{j=1}^{N}\Delta s_{\mathrm{L}}\sin\theta_{\mathrm{L}}(j)\left[\sum_{k=1}^{\min(i,j)}k_{\mathrm{SB}}(k)\right]. \tag{45}$$

Cable:

$$-\frac{1}{2}\frac{E_{\mathrm{C}}I_{\mathrm{C}}}{2\Delta s_{\mathrm{C}}}\left[\theta_{\mathrm{C}}(i+2)-\theta_{\mathrm{C}}(i)\right]-\sum_{j=1}^{i}\left[w_{\mathrm{C}}(j)+F_{y_{\mathrm{C}}}(j)\right]\Delta s_{\mathrm{C}}\cos\theta_{\mathrm{C}}(i)-F_{\mathrm{C}}\Delta s_{\mathrm{C}}\cos\theta_{\mathrm{C}}(i)-\sum_{j=1}^{i}f_{x_{\mathrm{C}}}(j)\Delta s_{\mathrm{C}}\sin\theta_{\mathrm{C}}(i)+P_0\Delta s_{\mathrm{C}}\sin\theta_{\mathrm{C}}(i)=0. \tag{46}$$

4.2 Solution technique

4.2.1 *Initial configuration*

The initial configuration is assumed to be a straight line lying on the seabed.

$$\theta_{\mathrm{L}}{}_i^{(1)}=0, \tag{47}$$

where, $\theta_{\mathrm{L}}{}_i^{(1)}$ is the initial SLWR's segment angle. Then, LWR is continuously bent under the action of buoyancy. In the buoyancy section, the SLWR's gravity can be obtained as:

$$w_{\mathrm{L}}(i)=w_{\mathrm{L}}(i)+\Delta w_{\mathrm{B}}. \tag{48}$$

4.2.2 *Recovery process*

First, a free catenary configuration with initial length L_{C} is established for cable. According to the free catenary equation (Trapper, 2020a), each section of the riser should meet the condition:

$$\frac{\mathrm{d}(\tan\theta_{\mathrm{C}})}{\mathrm{d}s_{\mathrm{C}}}=\frac{w_{\mathrm{C}}}{P_0}. \tag{49}$$

Ignoring the influence of the flexural rigidity of cable and considering the water depth d_{w} of the buoyancy, the relationship between the horizontal pulling force P_0 at the left end and other parameters can be obtained:

$$L_{\mathrm{C}}=\frac{P_0}{w_{\mathrm{C}}}\sinh\left[\operatorname{arcosh}\left(\frac{w_{\mathrm{C}}}{P_0}d_{\mathrm{w}}+1\right)\right]. \tag{50}$$

Solving Eq. (46) for P_0 at the initial configuration, then all other corresponding θ_{C} can be obtained by:

$$\theta_{\mathrm{C}}{}_i^{(1)}=2\pi-\arctan\left[\frac{w_{\mathrm{C}}}{P_0}(i-1)\Delta s_{\mathrm{C}}\right]. \tag{51}$$

By substituting θ_{C} into Eqs. (37) and (38), it would be possible to obtain cable initial configuration.

At this time, the free end coordinates of SLWR and cable are not equal in the x and y directions. The next step is to adjust P_0 and F_{C} considering the errors in the x and y directions by Eqs. (50) and (51). Thus, according to Eqs. (43) and (44), the new equilibrium configurations of SLWR and cable can be solved iteratively. As shown in Fig. 5, the condition for the iterative process stops if the errors in the$x$

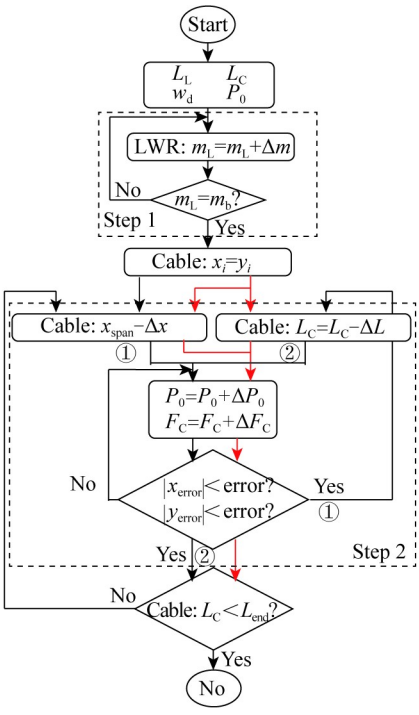

Fig. 5. Overall solution steps of the SLWR during abandonment and recovery (Red line: Method 2).

and y directions reach a given tolerance. The condition for the iterative process stops if the errors in the x and y directions reach a given tolerance.

$$P_0(i+1) = P_0(i) + \Delta P_0; \tag{52}$$

$$F_C(i+1) = F_C(i) + \Delta F_C, \tag{53}$$

where $P_0(i+1)$ and $F_C(i+1)$ represent the iterative update values of horizontal tension $P_0(i)$ and buoyancy $F_C(i)$, respectively.

4.2.3 *Newton-Raphson iterative algorithm*

The Newton-Raphson algorithm is an iterative algorithm for numerically finding the roots of nonlinear equations, and the nonlinear equation is:

$$u(x) = 0. \tag{54}$$

Let x_0 be the threshold value in [a, b], expand by Taylor formula and omit the quadratic term, approximately:

$$u(x) = u(x_0) + u'(x_0)(x - x_0). \tag{55}$$

Accordingly, the general iterative formula for finding the root is obtained:

$$x_{k+1} = x_k - u(x_k)/u'(x_k), \tag{56}$$

where $u'(x_k)$ is the derivative of the function $u(x)$ at x_k.

The numerical method in this paper only performs iterative solution updates through the rotation angle parameters θ^i. After clarifying the column vector F of the external force of the element and the tangent stiffness K of the integrated element, the Newton-Raphson iterative method is applied to solve $K\theta^i + F\theta^i = 0$, $(i = 1, \cdots, n)$.

$$\left(K + \frac{\mathrm{d}F}{\mathrm{d}\theta^i}\right)\Delta\theta^{i+1} = -K\theta^i - F\theta^i \tag{57}$$

with

$$\theta^{i+1} = \theta^i + \Delta\theta. \tag{58}$$

4.2.4 *Continuous installation process*

We can simulate the continuous installation process by periodically reducing the value of L_{span} and L_C. At each installation position, the static balance position is solved through the second step.

$$L_{span}(i+1) = L_{span}(i) + \Delta L_{span}; \tag{59}$$

$$L_C(i+1) = L_C(i) + \Delta L_C. \tag{60}$$

5 Validation and comparison

In this section, the validation and comparison are performed by an in-house written Matlab code, and the Orcaflex software version 10.3a (Orcina, 2015), which is a recognized software for global riser analysis in the market, is used to validate proposed model. For all the calculations we adopt the basic set of parameters as summarized in Table 1.

In order to verify the accuracy of the present model, the numerical results are compared with those of Orcaflex with the SLWR's segment number N_L=100 and cable's segment number N_C=60. The results of comparison between the present model and Orcaflex are shown in Fig. 6 at water depths 40, 600, 1160 and 1720 m. These depths are the distances between the seabed and the connection point of SLWR and cable, and these values equal to different $y(L_L)$, respectively.

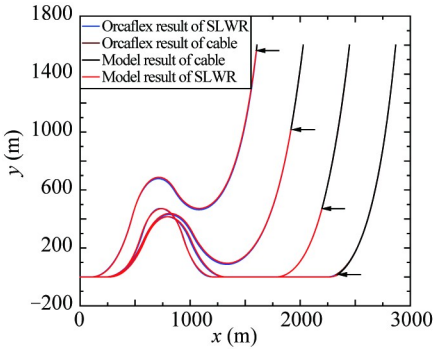

Fig. 6. Comparison between the present model and OrcaFlex.

It can be seen that the overall configurations of SLWR and cable from the present model are very consistent with those of Orcaflex. Table 2 shows the coordinate values and their error values between the present model and Orcaflex at the intersection point. An absolute error is 5.02 m in x direction with a relative error of 0.22%, and an absolute error is 5.31 m in y direction with a relative error of 0.33% for the intersection point. As to the maximum error between the present model and Orcaflex at the same node number, the maximum relative error is 1.22% at y direction with the water depth 40 m, which verifies the high accuracy of the present model.

6 Numerical analysis

During the recovery operation of the SLWR, there are two methods to complete this operation:

The first recovery method is to separate the movement of the vessel and the cable. As shown in Fig. 3, each step in the operation process corresponds to 1−6 in the figure. The

Table 2 Coordinates and errors between present model and OrcaFlex

	Water depth (m)	Present model (x, y) (m)	Orcaflex (x, y) (m)	Intersection error	Relative error (%)	Max. error (x, y) (m)	Relative error (%)
L_C (m)	1720	(2331.33, 10.61)	(2326.31, 15.95)	(5.02, 5.31)	(0.22, 0.33)	(9.38, 10.62)	(0.40, 0.66)
	1160	(2196.62, 468.73)	(2195.76, 468.68)	(0.86, 0.05)	(0.04, 0.00)	(8.50, 10.89)	(0.39, 0.68)
	600	(1914.00, 1010.77)	(1914.59, 1010.38)	(0.59, 0.39)	(0.03, 0.02)	(9.26, 18.16)	(0.48, 1.14)
	40	(1600.80, 1560.45)	(1601.86, 1560.31)	(1.06, 0.14)	(0.07, 0.01)	(11.59, 19.57)	(0.72, 1.22)

specific process is described as follows:

(1) Move the vessel to a given position.

(2) Recover the cable to a given length while keeping the vessel's position unchanged.

(3) Move the vessel to another given position while keeping the length of the cable unchanged.

(4) Repeat the above process of recovering the cable and moving the vessel until the flexible joint of SLWR reaches the water surface.

(5) Pass the towing cable from the platform to the vessel to start the transfer process.

The second recovery method is to realize the continuous recovery process of SLWR by moving the vessel and the cable at the same time. The specific process is described as follows:

(1) Move the vessel to a given position.

(2) The vessel is moving while the cable is being recovered.

(3) The movement velocity of the vessel is synchronized with the recovery velocity of the cable to avoid overstress of SLWR.

(4) Repeat the above process of recovering the cable and moving the vessel until the flexible joint of SLWR reaches the water surface.

(5) Pass the towing cable from the platform to the vessel to start the transfer process.

The first recovery method decouples the movement of the vessel from the operation of the winch, making the recovery operation easier to control. The second recovery method is relatively fast, but it must coordinate the movement velocity of the vessel and the recovery velocity of the cable. Both methods are feasible. In the comparison of the following calculation examples, we set the final shape of the SLWR and the cable to be consistent.

6.1 First and second recovery method

In the first recovery method, the vessel will move 120 m and then the cable is taken up by 160 m; and the vessel will move 120 m and the cable is taken up by 160 m at the same time in the second recovery method. Fig. 7 shows the configurations of SLWR and cable at different recovery steps for Methods 1 and 2. It can be clearly seen from the figure that in Method 1 the riser is lifted in a distributed manner, while in Method 2 it is a continuous process.

The distributions of bending moment, shear force and axial tension for different recovery steps are shown in Figs. 8−10. The numerical results of tension, bending moment, shear force and axial tension are calculated by Eqs. (26)−(28). It can be seen that the changes in its bending moment, shear force and axial tension in recovery Method 1 are not as continuous and regular as in recovery Method 2, which is determined by the characteristics of its installation method.

Fig. 11 shows the force change of the horizontal tension

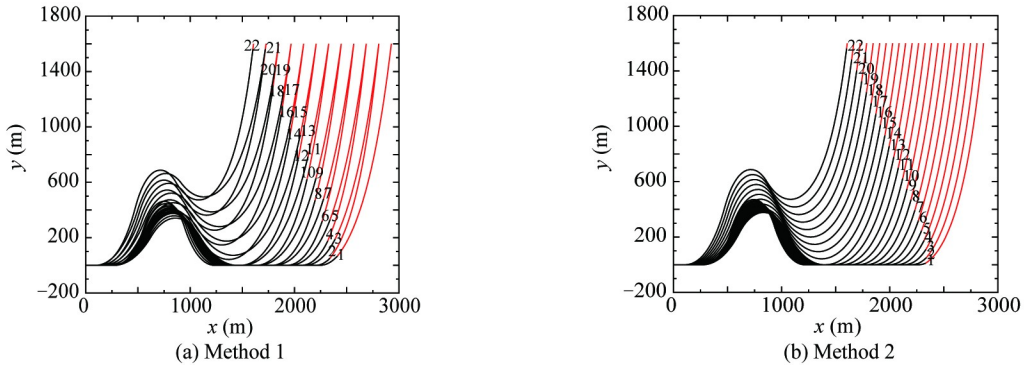

Fig. 7. Configurations of SLWR and cable at different recovery steps.

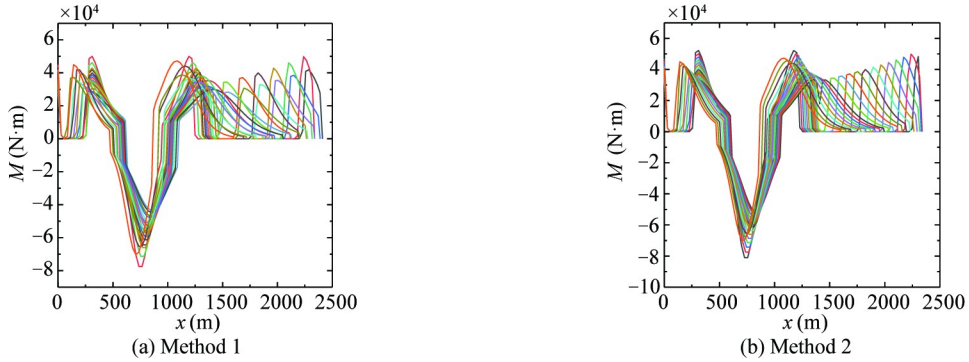

Fig. 8. Bending moment of SLWR at different recovery steps.

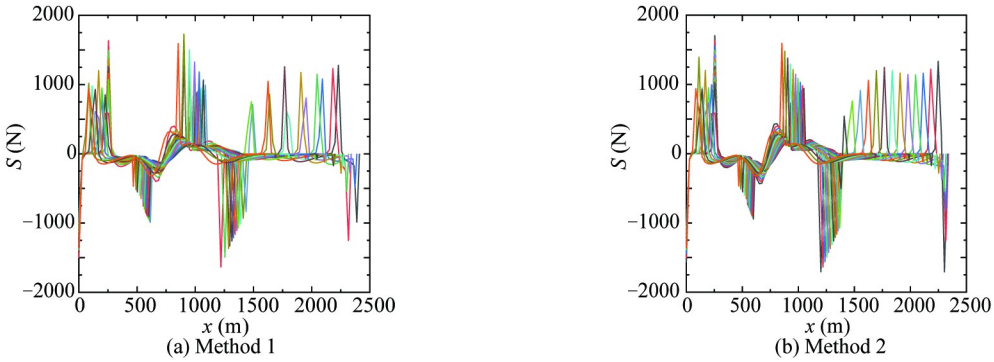

Fig. 9. Shear force of SLWR at different recovery steps.

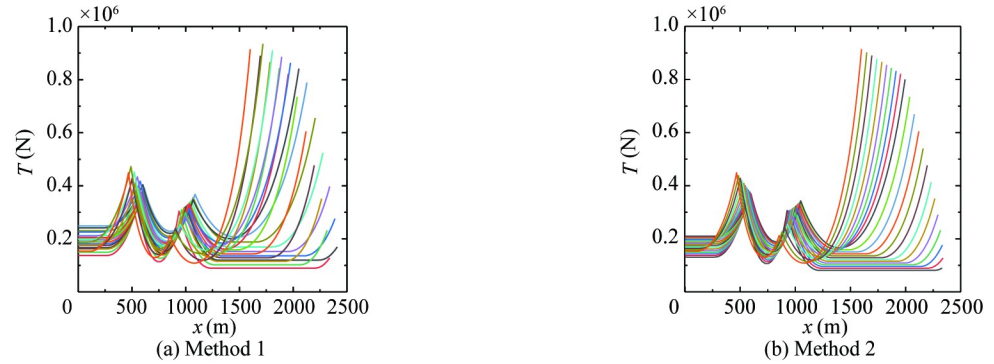

Fig. 10. Axial tension of SLWR at different recovery steps.

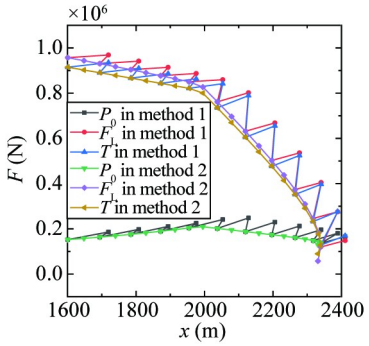

Fig. 11. P_0, T and F_L at right end of SLWR at different recovery steps.

P_0, the vertical tension F_L and the tension T at the right end (which is connected to the cable) of the SLWR concerning the x coordinate value of the right end of the SLWR during the entire recovery process. It can be seen that during the installation process of the first recovery method, there are procedural fluctuations of P_0, F_L and T, and the fluctuation value is relatively large. In the second recovery method, the P_0, F_L and T show approximately linear changes. At the moment when the SLWR leaves the seabed where x is about 2000 m, the slopes of P_0, F_L and T have changed significantly, and it is no longer approximately linear.

6.2 Third recovery method

In order to keep SLWR more stable and safer during the recovery process, the changing rate of forces P_0, F_L and T should be more linear. In DNV-OS-F101, it is stated that the tension of the riser needs to be kept "under control" to prevent damage to the pipe and coating by the load. If the tension change curve is stable and continuous, the riser is in a relatively safe condition as no sudden changes in tension have occurred during the recovery installation that could cause damage to the riser. One possible way is to change the ratio of the moving velocity of the installation vessel to the recovery velocity of cable when the SLWR leaves the seabed, so as to achieve an approximately linear changing ratio of the forces P_0, F_L, and T.

Hence, we introduce the parameters α and β. The parameter α represents the ratio of ship movement speed to cable recovery speed before the SLWR leaves the seabed. The parameter β represents the ratio of ship movement speed to cable recovery speed during the SLWR continues to lift after leaving the seabed. The speed ratios α and β are adjusted to optimize the recovery process by controlling the speed ratios α and β for different recovery stages, so that the riser morphology and the tube load of the recovery process are more uniform and continuous.

Fig. 12 shows the relationship between the tension with respect to the x-coordinate value of the right end of the SLWR before and after SLWR leaves the seabed at the same ratio, i.e., α=β. It can be seen that when the ratio gradually increases, the tension changing rate becomes slower. When α is equal to β, the tension change rate before SLWR

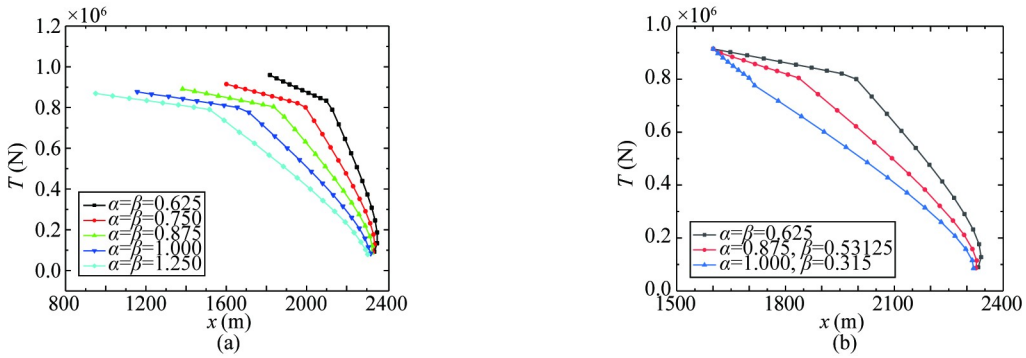

Fig. 12. Tension T at right end of SLWR and cable at different recovery steps for the same (a) and different (b) values of α and β.

leaves the seabed is always greater than the tension change rate after SLWR leaves the seabed. Therefore, we can appropriately increase the rate ratio α before leaving the seabed, as well as reduce the rate ratio β after leaving the seabed to keep the tension change more stable during the recovery process, which is defined as Method 3.

Method 3 is to adjust the values of α and β separately without changing the final shape to optimize the approximate linearization of the SLWR tension. Fig. 13 shows the tension with respect to the x-coordinate value at different combinations of α and β. It can be seen that with the increase of α and decrease of β, the tension changing rate will gradually approach to a straight line. When α=1 and β=0.315, it can be seen that the tension change rate has been approximately linear.

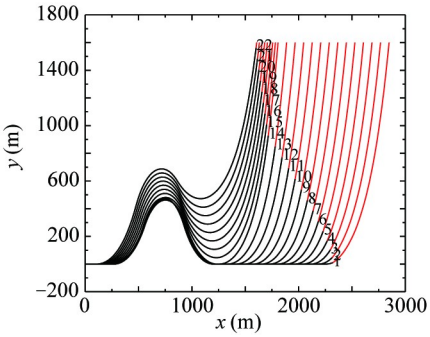

Fig. 13. Configurations of SLWR and cable at different recovery steps for Method 3.

Figs. 13−15 show the configuration, bending moment, shear force, and tension of SLWR during the recovery process in Method 3. It can be seen from Fig. 13 that before Step 14, the vessel moving velocity is the same as the cable recovery velocity due to α=1. After Step 14, the cable recovery velocity is significantly higher than the vessel moving velocity due to β=0.315.

6.3 Assessment criteria of the riser installation

Refer to the relevant standards and specifications (API Spec 17J, DNV-RP-F204 2010) for more detail. The ultimate limit states (ULS) in this part can be defined by maximum force and minimum bending radius (MBR). The maximum tension T_{max} and the maximum bending moment M_{max} can be calculated by the following formulas:

$$T_{max} = (A_o - A_i)\sigma_a C_s; \tag{61}$$

$$M_{max} = \frac{2I\sigma_m}{D} \cdot C_s, \tag{62}$$

where A_o and A_i represent the cross-sectional area of the outer and inner riser respectively, I is the moment of inertia, and C_s is safety factor. According to the international standard *API Spec 17J*, the value of C_s is 0.67.

In general, the total axial stress of the metal pipe is adopted to estimate the riser fatigue damage, which is a linear combination of the axial stress σ_a contributed by wall tension and bending stress σ_m contributed by bending moment

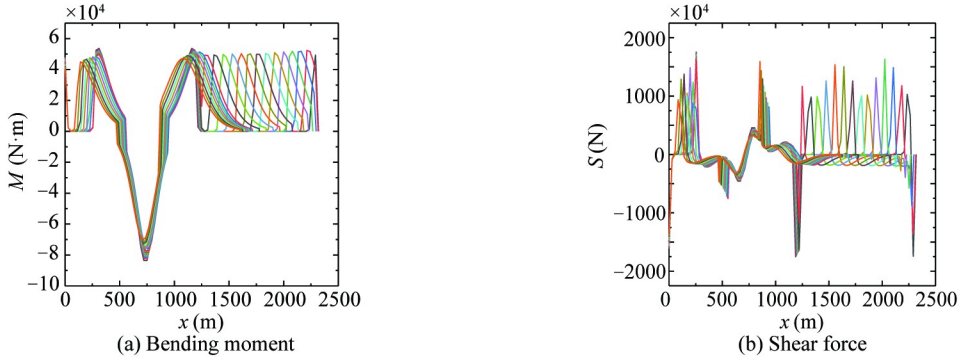

Fig. 14. Bending moment and shear force of SLWR at different recovery steps for Method 3.

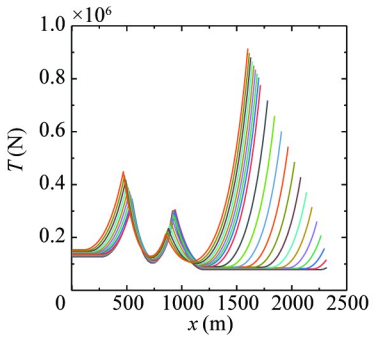

Fig. 15. Tension of SLWR at different recovery steps for Method 3.

(DNV-RP-F204 2010). The maximum values of σ_a and σ_m are given by the following formulas:

$$\sigma_a = \frac{T_{max}}{A_o - A_i}, \sigma_m = \frac{|M_{max}|D}{2I}. \tag{63}$$

The calculated maximum allowable tension is T_{max}= 1430.89 kN, and the maximum allowable bending moment is M_{max} =83.3 kN·m. According to Fig. 14 and Fig. 15, the maximum tension obtained by Method 3 is about 910 kN and the maximum bending moment is 82.1 kN·m. In Fig. 16, the maximum tension and maximum bending moment of Method 3 are within the allowable range. The maximum tension and maximum bending moment of Method 3 are within the allowable range.

When the bending radius is less than the minimum bending radius, the material will crack, and exceed the maximum bending moment. Therefore, the bending radius under the maximum bending moment condition is considered as the minimum bending radius, and is defined by the minimum bending curvature:

$$\frac{1}{\rho_{min}} = \frac{M_{max}}{EI}, \tag{64}$$

where, ρ is bending curvature, and ρ_{min}=0.00883.

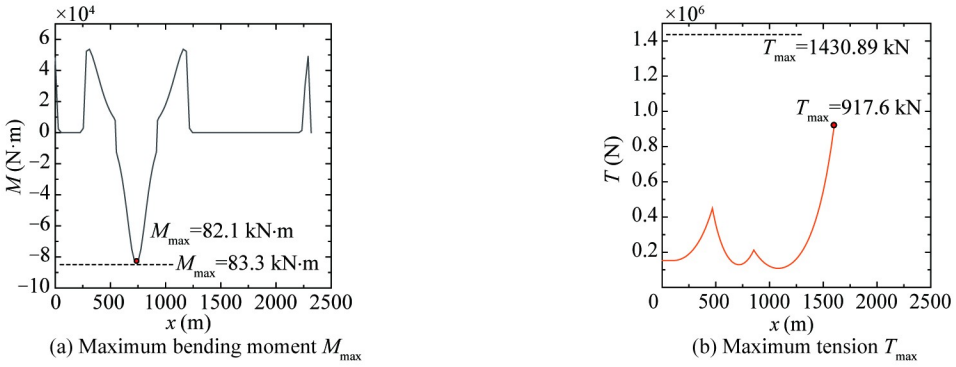

Fig. 16. Maximum bending moment M_{max} and tension T_{max} of SLWR for Method 3.

7 Conclusions

This paper conducts an evaluation of abandonment and recovery operation of steel lazy-wave riser in deepwater. The conclusions are drawn as follows.

The numerical analysis method in this paper is summarized as constructing the coupled static equilibrium equation of SLWR and cable by using the principle of minimum total potential energy, and further implementing the finite difference method and Newton-Raphson iterative algorithm to solve the differential equation. Through validation and comparison, it is verified that the present numerical results are very consistent with those of Orcaflex.

Three recovery methods of the installation operation are performed to evaluate the rate ratio of the vessel's moving velocity to cable's recovery velocity during the abandonment and recovery operation. The main difference between these methods is the ratio (α or β) before or after the SLWR leaves the seabed. The following results are obtained from the analysis.

(1) During the installation process, axial tension, horizontal tension and vertical buoyancy present fluctuations in the first method, whereas they show approximately linear changes in the second method. When the SLWR leaves the seabed, the slopes of these forces have changed significantly, and it is no longer approximately linear.

(2) When the ratio of the vessel's moving velocity to cable's recovery velocity gradually increases, the tension changing rate becomes slower. The tension change rate before SLWR leaves the seabed is always greater than that after SLWR leaves the seabed in Method 2.

(3) In order to keep the tension change more stable during the recovery process, the rate ratio before leaving the seabed is increased, while the rate ratio after leaving the seabed is reduced. When α=1 and β=0.315, the tension change rate has been approximately linear in Method 3.

References

Cabrera-Miranda, J.M. and Paik, J.K., 2019. Two-phase flow induced vibrations in a marine riser conveying a fluid with rectangular pulse train mass, *Ocean Engineering*, 174, 71–83.

Chatjigeorgiou, I.K., 2004. On the parametric excitation of vertical

elastic slender structures and the effect of damping in marine applications, *Applied Ocean Research*, 26(1–2), 23–33.

Chen, L.L., Gu, J.J., Jia, J.C., Gao, L. and Wang, S.J., 2023. Numerical analysis of configuration for steel lazy-wave riser in deepwater, *Ships and Offshore Structures*, 18(2), 285–301.

Chen, W.M., Guo, S.X., Li, Y.L., Gai, Y.X. and Shen, Y.J., 2021. Structural configurations and dynamic performances of flexible riser with distributed buoyancy modules based on FEM simulations, *International Journal of Naval Architecture and Ocean Engineering*, 13, 650–658.

Cheng, Y., Tang, L.Y. and Fan, T.H., 2020. Dynamic analysis of deepwater steel lazy wave riser with internal flow and seabed interaction using a nonlinear finite element method, *Ocean Engineering*, 209, 107498.

Dow, J.O., 1999. Principle of minimum potential energy, in: Dow, J.O. (ed.), *A Unified Approach to the Finite Element Method and Error Analysis Procedures*, , 9–20.

Gu, J.J., Ma, T.Q., Chen, L.L., Jia, J.C. and Kang, K., 2021. Dynamic analysis of deepwater risers conveying two-phase flow under vortex-induced vibration, *Journal of the Brazilian Society of Mechanical Sciences and Engineering*, 43(4), 188.

Hoffman, J., Clausing, K., Robinson, S., Subramanian, P. and Zummo, A., 2017. The stones project: subsea, umbilical, riser and flowline systems, *Proceedings of Offshore Technology Conference*, Houston, 1–20.

Hoffman, J.D. and Frankel, S., 2001. *Numerical Methods for Engineers and Scientists*, second Ed., CRC Press, Boca Raton.

Ismail-Zadeh, A. and Tackley, P., 2010. Finite difference method, in: Ismail-Zadeh, A. and Tackley, P. (eds.), *Computational Methods for Geodynamics*, Cambridge University Press, Cambridge, pp. 24–42.

Jensen, G.A., Säfström, N., Nguyen, T.D. and Fossen, T.I., 2010. A nonlinear PDE formulation for offshore vessel pipeline installation, *Ocean Engineering*, 37(4), 365–377.

Kim, S. and Kim, M.H., 2015. Dynamic behaviors of conventional SCR and lazy-wave SCR for FPSOs in deepwater, *Ocean Engineering*, 106, 396–414.

Kuiper, G.L., Brugmans, J. and Metrikine, A.V., 2008. Destabilization of deep-water risers by a heaving platform, *Journal of Sound and Vibration*, 310(3), 541–557.

Morison, J.R., Johnson, J.W. and Schaaf, S.A., 1950. The force exerted by surface waves on piles, *Journal of Petroleum Technology*, 2(5), 149–154.

Oh, J., Jung, D., Kim, H., Min, C. and Cho, S., 2020. A study on the simulation-based installation shape design method of steel lazy wave riser (SLWR) in ultra deepwater depth, *Ocean Engineering*, 197, 106902.

Orcina, 2015. *Orcaflex QA*, *Testing and Validation*, Document 99/005: 7, Orcina Ltd., Cumbria.

Randolph, M.F., Gaudin, C., Gourvenec, S.M., White, D.J., Boylan, N. and Cassidy, M.J., 2011. Recent advances in offshore geotechnics for deep water oil and gas developments, *Ocean Engineering*, 38(7), 818–834.

Ruan, W.D., Shi, J.C., Sun, B. and Qi, K.F., 2021. Study on fatigue damage optimization mechanism of deepwater lazy wave risers based on multiple waveform serial arrangement, *Ocean Engineering*, 228, 108926.

Surana, K.S. and Reddy, J.N., 2016, Linear elasticity using the principle of minimum total potential energy, in: Surana, K.S. and Reddy, J.N. (eds.), *The Finite Element Method for Boundary Value Problems*, CRC Press, Boca Raton, pp. 609–624.

Thomas, B., Benirschke, A. and Sarkar, T., 2010. Parque das Conchas (BC-10) steel lazy wave riser installation: pre-abandonment, recovery and transfer challenges, *Proceedings of Offshore Technology Conference*, Houston, 1224–1235.

Trapper, P.A., 2019. Feasible numerical method for analysis of offshore pipeline in installation, *Applied Ocean Research*, 88, 48–62.

Trapper, P.A., 2020a. Feasible numerical analysis of steel lazy-wave riser, *Ocean Engineering*, 195, 106643.

Trapper, P.A., 2020b. Static analysis of offshore pipe-lay on flat inelastic seabed, *Ocean Engineering*, 213, 107673.

Trapper, P.A. and Mishal, I., 2020. Numerical analysis of offshore pipe-lay subjected to environment-induced non-uniformly distributed follower loads, *Applied Ocean Research*, 100, 102149.

Wang, J.L. and Duan, M.L., 2015. A nonlinear model for deepwater steel lazy-wave riser configuration with ocean current and internal flow, *Ocean Engineering*, 94, 155–162.

Wang, J.L., Duan, M.L. and He, R.Y., 2018. A nonlinear dynamic model for 2D deepwater steel lazy-wave riser subjected to top–end imposed excitations, *Ships and Offshore Structures*, 13(3), 330–342.

Wang, J.L., Duan, M.L., He, T. and Jing, C., 2014. Numerical solutions for nonlinear large deformation behaviour of deepwater steel lazy-wave riser, *Ships and Offshore Structures*, 9(6), 655–668.

Wang, J.L., Duan, M.L. and Luo, J.M., 2015a. Mathematical model of steel lazy-wave riser abandonment and recovery in deepwater, *Marine Structures*, 41, 127–153.

Wang, J.L., Duan, M.L., Wang, Y., Li, X.Z. and Luo, J.M., 2015b. A nonlinear mechanical model for deepwater steel lazy-wave riser transfer process during installation, *Applied Ocean Research*, 50, 217–226.

Xu, Y.X., Fang, P. and Bai, Y., 2021. Mechanical behavior of metallic strip flexible pipes during reeling operation, *Marine Structures*, 77, 102942.

Yang, H.Z. and Li, H.J., 2011. Sensitivity analysis of fatigue life prediction for deepwater steel lazy wave catenary risers, *Science China Technological Sciences*, 54(7), 1881–1887.